

Unconditionally Stable Time Stepping Method for Mixed Finite Element Maxwell Solvers

Zane D. Crawford^{1, 2, *}, Jie Li¹, Andrew Christlieb², and Balasubramaniam Shanker¹

Abstract—Time domain finite element methods (TD-FEM) for computing electromagnetic fields are well studied. TD-FEM solution is typically effected using Newmark-Beta methods. One of the challenges of TD-FEM is the presence of a DC null-space that grows with time. This can be overcome by solving Maxwell equations directly. One approach, called time domain mixed finite element method (TD-MFEM), discretizes Maxwell’s equations using appropriate spatial basis sets and leapfrog time stepping. Typically, the basis functions used to discretize field quantities have been low order. It is conditionally stable, and there is a strong link between time step size and mesh dependent eigenvalues, much like the Courant-Friedrichs-Lewy (CFL) condition. This implies that the time step sizes can be very small. To overcome this challenge, we use the Newmark-Beta approach. The principal contribution of this work is the development of, and rigorous proof of, unconditional stability for higher order TD-MFEM for different boundary conditions. Further, we analyze nullspaces of the resulting system, and demonstrate stability and convergence. All results are compared against the conditionally stable leapfrog approach.

1. INTRODUCTION

Efficient solutions to Maxwell’s equations is of significant interest to problems in fields ranging from microwave engineering to optics to radar to remote sensing to plasma physics [1–5]. As a result, it has seen extensive development over the past four decades. So much so that there exist reliable commercial simulators that are trusted for design and analysis; to wit, most microwave engineering and antenna design is carried out on a laptop before being fabricated and tested. Despite these advances, there are a number of open problems and challenges, largely brought on by our desire to improve the fidelity of simulation for increasingly complex geometric and material layouts. Adding temporal dimension to the analysis increases the challenges as well. The methods used for solution to Maxwell’s equations are based either on differential or integral equations; this paper will focus on the former.

Over the years, differential equation based methods have become the mainstay of computational electromagnetic tools, starting with the classical Yee-algorithm for direct discretization of Maxwell’s equations [6] to finite element methods (FEMs) [7, 8]. A number of challenges had to be overcome to make FEMs robust and viable for the use in design and analysis of systems [9, 10]. Over the years, research on FEM has focused on developing methods so as to increase the accuracy and reduce computational costs; these include higher order interpolatory basis functions [11], higher order hierarchical basis sets [12], and domain decomposition methods [13]. These techniques have largely been applied to solving the vector wave equation in the frequency domain. In the time domain, the temporal discretization follows a Newmark-Beta prescription [14, 15]. With the right choice of parameters, it has been shown that this prescription is unconditionally stable. The time step size is not intimately tied to the smallest mesh feature, but chosen to capture the physics to a prescribed order. However, the

Received 10 February 2020, Accepted 29 May 2020, Scheduled 16 June 2020

* Corresponding author: Zane Crawford (crawf326@msu.edu).

¹ Department of Electrical and Computer Engineering, Michigan State University, East Lansing, MI, USA. ² Department of Computational Science, Mathematics, and Engineering, Michigan State University, East Lansing, MI, USA.

solutions to the vector wave equation are prone to inaccuracies arising from a non-trivial null space that corresponds to a function of the form $t\nabla\phi(\bar{r})$, where $\phi(\bar{r})$ is a scalar function of space.

There has been an effort to use finite elements to directly solve Maxwell's equations [16–18], *albeit* less so than vector wave formulations. These methods follow the prescription of the Yee-algorithm. Faraday's and Ampere's laws are staggered in time leading to a leap frog time stepping. As a result, they do not have a time-growing null space, are conditionally stable, and energy conserving. Unfortunately, the time step size depends on the size of the features of the mesh and materials defined within it. The resulting time step sizes are very small, significantly more so than needed to represent content at the highest frequency. This is in contrast to the state of the art of solving the vector wave equation.

It would be ideal if one could render TD-MFEM provably unconditionally stable (it would enable reaping the advances made for vector wave equation FEM solvers). Earlier work has analyzed the stability for leapfrog time stepping in TD-MFEM [19]. Likewise, unconditionally stable time stepping schemes have been used in TD-MFEM, but without any rigorous analysis to prove stability [20]. In this work, we will prove that using Newmark-Beta method for TD-MFEM can produce unconditionally stable time stepping schemes that are up to second order accurate in time. With the correct choice in parameters, the time stepping schemes are shown to be energy conserving and non-dissipative. Furthermore, these properties hold for higher-order spatial basis functions used to discretize TD-MFEM. Thus, the specific contributions of this work are (i) a general framework for creating time stepping schemes of up to second order for the TD-MFEM of arbitrary spatial order, (ii) proof of stability for different boundary conditions and error analysis for the time stepping scheme, (iii) analysis of the null space of the discrete system, and (iv) numerical results verifying the analytic proofs.

The rest of the paper is organized as follows. Section 2 describes the general problem. Section 3 presents the spatial and temporal discretization of Maxwell's equations. This section contrasts the Newmark-Beta method to the leapfrog method and provides stability and error analysis of the Newmark-Beta method applied to the MFEM. Section 4 presents several numerical results verifying properties discussed in previous sections and the overall efficacy of the method. Finally, conclusion and other remarks are provided in Section 5.

2. PROBLEM STATEMENT

Consider the volume $\Omega \in \mathbb{R}^3$ bounded by Γ shown in Figure 1. In this domain, assume that the region has homogeneous, isotropic, and time-independent constitutive parameters, denoted by ε (F/m) for the permittivity and μ (H/m) for the permeability. Assume that the volume is source free, being free of impressed charges or currents. The magnetic field $\bar{H}(\bar{r}, t)$ (A/m) and electric flux density $\bar{D}(\bar{r}, t)$ (C/m²) are defined in terms of the magnetic flux density $\bar{B}(\bar{r}, t)$ (Wb/m²) and electric field $\bar{E}(\bar{r}, t)$ (V/m), respectively, through the constitutive parameters such that

$$\bar{H}(\bar{r}, t) = \mu^{-1}\bar{B}(\bar{r}, t) \quad (1a)$$

$$\bar{D}(\bar{r}, t) = \varepsilon\bar{E}(\bar{r}, t). \quad (1b)$$

The electric field and magnetic flux density are governed by Maxwell's equations

$$\begin{aligned} \frac{\partial \bar{B}(\bar{r}, t)}{\partial t} &= -\nabla \times \bar{E}(\bar{r}, t) \\ \frac{\partial \varepsilon \bar{E}(\bar{r}, t)}{\partial t} &= \nabla \times \frac{\bar{B}(\bar{r}, t)}{\mu} \end{aligned} \quad (2)$$

$$\nabla \cdot (\varepsilon \bar{E}(\bar{r}, t)) = 0$$

$$\nabla \cdot \bar{B}(\bar{r}, t) = 0.$$

The boundary Γ may be partitioned into several subdomains, Γ_i , such that $\Gamma := \cup_i \Gamma_i$. Each Γ_i has a boundary condition, either Dirichlet (Γ_D), Neumann (Γ_N), or impedance (Γ_I) [10]. The boundary conditions are defined as

$$\hat{n} \times \bar{E}(\bar{r}, t) = \Psi_D(\bar{r}, t) \quad \text{on } \Gamma_D \quad (3a)$$

$$\hat{n} \times \frac{\bar{B}(\bar{r}, t)}{\mu} = \Psi_N(\bar{r}, t) \quad \text{on } \Gamma_N \quad (3b)$$

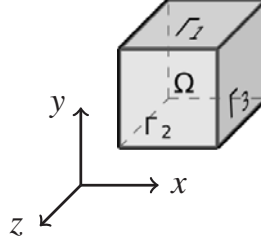


Figure 1. Sample volume Ω with different boundary conditions.

$$\hat{n} \times \frac{\bar{B}(\bar{r}, t)}{\mu} - Y \hat{n} \times \hat{n} \times \bar{E}(\bar{r}, t) = \Psi_I(\bar{r}, t) \quad \text{on } \Gamma_I \quad (3c)$$

where $Y = \sqrt{\varepsilon/\mu}$ (\mathcal{U}) is the surface admittance. The functions $\Psi_D(\bar{r}, t)$, $\Psi_N(\bar{r}, t)$, and $\Psi_I(\bar{r}, t)$ represent some arbitrary functions defined by the user. Additionally, we assume that initial conditions on the fields, $\bar{E}(\mathbf{r}, 0)$ and $\bar{B}(\mathbf{r}, 0)$, satisfy Eq. (2).

3. MFEM FORMULATION

3.1. Variational Formulation

Solutions to Eq. (2) are found by creating variational equations with appropriate function spaces. The suitable function space for the electric field is the Hilbert space

$$H(\text{curl}; \Omega) = \{\bar{u} \in \bar{L}^2(\Omega); \nabla \times \bar{u} \in \bar{L}^2(\Omega)\}, \quad (4)$$

which ensures that the tangential component of the field is continuous across tetrahedral faces. Likewise, the Hilbert space

$$H(\text{div}; \Omega) = \{\bar{u} \in \bar{L}^2(\Omega); \nabla \cdot \bar{u} \in L^2(\Omega)\} \quad (5)$$

is used for the magnetic flux density, which permits functions that have normal continuity across tetrahedral faces. The Whitney edge basis function and Whitney face basis function reside in $H(\text{curl}; \Omega)$ and $H(\text{div}; \Omega)$, respectively, and can be used to discretize the fields [16]. The variational equations are formed by taking inner products of Faraday's law with the Whitney face basis function \bar{B}^* and Ampere's law with the Whitney edge basis function \bar{E}^* such that

$$\int d\Omega \frac{1}{\mu} \frac{\partial}{\partial t} \bar{B} \cdot \bar{B}^* = - \int d\Omega \frac{1}{\mu} \nabla \times \bar{E} \cdot \bar{B}^*, \quad (6a)$$

$$\int d\Omega \varepsilon \frac{\partial}{\partial t} \bar{E} \cdot \bar{E}^* = \int d\Omega \nabla \times \frac{1}{\mu} \bar{B} \cdot \bar{E}^*. \quad (6b)$$

3.2. Spatial Discretization

The spatial discretization is obtained by applying Galerkin's method to the variational equations. As previously stated, Whitney edge and face elements as seen in [16] define the lowest order representation of \bar{E}^* and \bar{B}^* . The electric field is represented using Whitney edge elements and the magnetic flux using Whitney face elements such that

$$\bar{E}(\bar{r}, t) = \sum_{i=1}^{N_e} e_i(t) \bar{W}_i^1(\bar{r}), \quad \bar{B}(\bar{r}, t) = \sum_{i=1}^{N_f} b_i(t) \bar{W}_i^2(\bar{r}), \quad (7)$$

where N_e is the number of edges, and N_f is the number of faces. It is natural to use higher order basis function for more accuracy. We use the interpolatory higher order basis functions defined in [11] for Whitney edge elements and for Whitney face elements defined in [12]. We define vectors $\bar{e} = [e_1(t), e_2(t), \dots, e_{N_e}(t)]^T$ and $\bar{b} = [b_1(t), b_2(t), \dots, b_{N_f}(t)]^T$ that have the degrees of freedom $e_i(t)$

and $b_i(t)$ as elements. Using the defined expansion for the field and flux quantities, applying the Galerkin method to Eq. (6) yields the semi-discrete Maxwell's equations

$$\begin{aligned}\frac{\partial \mathbf{M}_{\mu-1} \bar{b}}{\partial t} &= -\mathbf{M}_c \bar{e} \\ \frac{\partial \mathbf{M}_\varepsilon \bar{e}}{\partial t} &= \mathbf{M}_c^T \bar{b} - \mathbf{M}_I \bar{e} + \bar{j}_N + \bar{j}_I.\end{aligned}\quad (8)$$

Here, the matrices are defined as

$$[\mathbf{M}_\varepsilon]_{i,j} = \int_{\Omega} d\Omega \varepsilon \bar{W}_i^1(\bar{r}) \cdot \bar{W}_j^1(\bar{r}), \quad (9a)$$

$$[\mathbf{M}_{\mu-1}]_{i,j} = \int_{\Omega} d\Omega \frac{1}{\mu} \bar{W}_i^2(\bar{r}) \cdot \bar{W}_j^2(\bar{r}), \quad (9b)$$

$$[\mathbf{M}_c]_{i,j} = \int_{\Omega} d\Omega \frac{1}{\mu} \bar{W}_i^2(\bar{r}) \cdot \nabla \times \bar{W}_j^1(\bar{r}), \quad (9c)$$

$$[\mathbf{M}_c^T]_{i,j} = \int_{\Omega} d\Omega \frac{1}{\mu} \bar{W}_j^2(\bar{r}) \cdot \nabla \times \bar{W}_i^1(\bar{r}), \quad (9d)$$

$$[\mathbf{M}_I]_{i,j} = \int_{\Gamma_I} d\Gamma Y \hat{n} \times \bar{W}_i^1(\bar{r}) \cdot \hat{n} \times \bar{W}_j^1(\bar{r}). \quad (9e)$$

The elements of the coefficient vectors \bar{j}_N and \bar{j}_I are defined as

$$\begin{aligned}\bar{j}_N]_i(t) &= \int_{\Gamma_N} d\Gamma_N \bar{W}_i^1(\bar{r}) \cdot \Psi_N(\bar{r}, t) \\ \bar{j}_I]_i(t) &= \int_{\Gamma_I} d\Gamma_I \bar{W}_i^1(\bar{r}) \cdot \Psi_I(\bar{r}, t)\end{aligned}\quad (10)$$

and represent the boundary current due to Neumann and impedance boundary conditions. Another interpretation of the TD-MFEM is through discrete exterior calculus. The Galerkin discrete Hodge matrices \mathbf{M}_ε and $\mathbf{M}_{\mu-1}$ are defined as [21]. The discrete curl operator \mathbf{D}_c is defined as

$$\mathbf{D}_c = \frac{1}{\mu} \mathbf{M}_{\mu-1}^{-1} \mathbf{M}_c. \quad (11)$$

The discrete curl operator and its transpose for the lowest order maps edges of a tetrahedron to the faces it bounds, as well as preserves the direction of the curl on that face [22]. This follows from the concept of the exterior derivative in the generalized Stokes theorem from exterior calculus. Equation (11) holds for all orders, however only has a simple mapping of faces to edges for the lowest order.

3.3. Temporal Discretization

The semi-discrete Maxwell's equations, derived in the previous section, are fully discretized by choosing an appropriate temporal discretization. Discretization schemes exist which solve the electric field and magnetic flux density concurrently or in a staggered fashion. In a staggered scheme, the solutions to Faraday's law and Ampere's law lie at different time steps, which allows a different time stepping method for each equation. A concurrent time stepping scheme couples the equations into a single system, written in the form

$$\begin{bmatrix} \mathbf{I} & 0 \\ 0 & \mathbf{M}_\varepsilon \end{bmatrix} \begin{bmatrix} \partial_t \bar{b} \\ \partial_t \bar{e} \end{bmatrix} + \begin{bmatrix} 0 & \mathbf{D}_c \\ -\mathbf{D}_c^T \mathbf{M}_{\mu-1} & \mathbf{M}_I \end{bmatrix} \begin{bmatrix} \bar{b} \\ \bar{e} \end{bmatrix} = \begin{bmatrix} 0 \\ \bar{j}_N + \bar{j}_I \end{bmatrix}, \quad (12)$$

where \mathbf{I} is the identity matrix. The single time derivative allows for the choice of a single time stepping scheme and implies that the solved quantities lie at the same time step. The following subsections discuss the leapfrog method (for the sake of completeness) and the Newmark-Beta method and their applications to finding solutions to the semi-discrete Maxwell's equations. Note that time step sizes for leapfrog ($\Delta_{t,LF}$) and Newmark-Beta ($\Delta_{t,N\beta}$) will be different.

3.3.1. Leapfrog Method

In the leapfrog method, the time derivatives in Faraday's law and Ampere's law are discretized using central finite differences staggered at half-time step intervals. Applying this to Eq. (8) yields

$$\bar{b}^{n+\frac{1}{2}} = \bar{b}^{n-\frac{1}{2}} - \Delta_{t,LF} \mathbf{D}_c \bar{e}^n \quad (13a)$$

$$(\mathbf{M}_\varepsilon + \mathbf{M}_I) \bar{e}^{n+1} = \mathbf{M}_\varepsilon \bar{e}^n + \Delta_{t,LF} \mathbf{D}_c^T \mathbf{M}_{\mu^{-1}} \bar{b}^{n+\frac{1}{2}} + \Delta_{t,LF} \left(\bar{j}_N^{n+\frac{1}{2}} + \bar{j}_I^{n+\frac{1}{2}} \right). \quad (13b)$$

The time stepping scheme consists of an explicit update in Faraday's law and a matrix inversion in Ampere's law as the Galerkin Hodge matrix is sparse, but not diagonal. It is conditionally stable [23, 24] provided that time step size satisfies

$$\Delta_{t,LF} \leq \frac{2}{\sqrt{\rho(\mathbf{M}_\varepsilon^{-1} \mathbf{D}_c^T \mathbf{M}_{\mu^{-1}} \mathbf{D}_c)}}. \quad (14)$$

When the time step size satisfies the stability requirement, the time stepping scheme also conserves energy. The mesh that discretizes the volume Ω determines the maximum time step size. The spectral radius of the matrices tends to grow as elements in the mesh shrink, limiting the time step size in relation to the maximum frequency the mesh could resolve.

3.3.2. Spectral Radius

One drawback of this time-stepping scheme is that its stability is tied to the discretization of the mesh and the dielectric and magnetic material within Ω . As the electrical size of the elements shrinks, so does the maximum time step size, regardless of coarser features of the mesh.

In Table 1, the relationships between the edge lengths h , spectral radius λ_{\max} , and time step sizes $\Delta_{t,LF}$ for the leapfrog scheme are presented. The spectral radius increases as the edge lengths shrink, resulting in a smaller maximum time step. Instead, it is preferred that time step is dictated by the bandwidth of the signals present in the simulation. In the results, it will show that the spatial errors tend to dominate error far more than temporal error, especially for the lowest order spatial basis functions.

Table 1. Leapfrog maximum time-step vs mesh edge lengths.

λ_{\max}	$c\Delta_{t,LF}$	h_{\max}	h_{avg}	h_{\min}
1.0587E+03	6.1468E-02	5.0000E-01	3.2400E-01	1.9376E-01
2.5661E+03	3.9481E-02	3.2773E-01	2.1477E-01	1.3689E-01
6.4293E+03	2.4943E-02	2.2165E-01	1.4365E-01	7.8437E-02
9.8165E+03	2.0186E-02	1.6865E-01	1.0925E-01	5.7826E-02
1.2769E+02	1.7699E-01	1.4142E+00	1.0424E+00	8.5782E-01
2.3979E+02	1.2916E-01	1.5326E+00	8.8836E-01	4.2409E-01
1.4249E+03	5.2983E-02	1.4142E+00	5.6001E-01	1.8142E-01
1.1535E+04	1.8622E-02	1.4142E+00	2.2648E-01	6.2023E-02

3.3.3. Newmark-Beta

The Newmark-Beta method is a concurrent time stepping method to solve second order differential equations [25, 26] and is a popular method of choice for solving TD-FEM. To begin, the first order differential equation from Eq. (12) is recast as a second order differential equation,

$$\mathbf{A}_2 \partial_t^2 \bar{u} + \mathbf{A}_1 \partial_t \bar{u} + \mathbf{A}_0 \bar{u} + \bar{f} = 0, \quad (15)$$

where

$$\begin{aligned} \bar{\mathbf{u}} &= \begin{bmatrix} \bar{\mathbf{b}} \\ \bar{\mathbf{e}} \end{bmatrix}, \quad \bar{\mathbf{f}} = \begin{bmatrix} 0 \\ -(\bar{j}_I + \bar{j}_N) \end{bmatrix}, \\ \mathbf{A}_2 &= 0, \quad \mathbf{A}_1 = \begin{bmatrix} \mathbf{I} & 0 \\ 0 & \mathbf{M}_\varepsilon \end{bmatrix}, \quad \mathbf{A}_0 = \begin{bmatrix} 0 & \mathbf{D}_c \\ -\mathbf{D}_c^T \mathbf{M}_{\mu^{-1}} & \mathbf{M}_I \end{bmatrix}. \end{aligned} \quad (16)$$

Applying a 1-dimensional finite element method in time and identifying particular weights in the formulation results in a three-step recurrence relation that uses two parameters to yield different accuracy and stability properties [27]. The three-step recurrence relation for Eq. (16) is defined as

$$\begin{aligned} & [\gamma \mathbf{A}_1 + \beta \Delta_{t,N\beta} \mathbf{A}_0] \bar{\mathbf{u}}^{n+1} + \left[(1 - 2\gamma) \mathbf{A}_1 + \left(\frac{1}{2} + \gamma - 2\beta \right) \Delta_{t,N\beta} \mathbf{A}_0 \right] \bar{\mathbf{u}}^n \\ & + \left[(\gamma - 1) \mathbf{A}_1 + \left(\frac{1}{2} - \gamma + \beta \right) \Delta_{t,N\beta} \mathbf{A}_0 \right] \bar{\mathbf{u}}^{n-1} \\ & + (\beta \Delta_{t,N\beta}) \bar{\mathbf{f}}^{n+1} + \left(\frac{1}{2} + \gamma - 2\beta \right) \Delta_{t,N\beta} \bar{\mathbf{f}}^n + \left(\frac{1}{2} - \gamma + \beta \right) \Delta_{t,N\beta} \bar{\mathbf{f}}^{n-1} = 0 \end{aligned} \quad (17)$$

which has the degrees of freedom for the electric field and magnetic flux density at the same time step. The parameters γ and β affect the accuracy and stability properties. The following sections prove and demonstrate that with appropriate choice of parameters, the TD-MFEM system with Dirichlet, Neumann, and impedance boundary conditions is not only unconditionally stable, but also energy conserving.

3.4. Stability Analysis

In order to determine the stability of the Newmark-Beta time-stepping scheme, the zero-input response of the system is examined using a z -transform. For the system to be stable, the roots of the z -transformed scheme must lie on or within the unit circle in the complex plane. The spectral theorem is used on Eq. (17) such that the matrix $\mathbf{A}_1^{-1} \mathbf{A}_0$ is replaced by its eigenvalue λ [10, 28]. Taking the z -transform yields the quadratic equation

$$\begin{aligned} & \left([\gamma + \beta \Delta_{t,N\beta} \lambda] z^2 + \left[(1 - 2\gamma) + \left(\frac{1}{2} + \gamma - 2\beta \right) \Delta_{t,N\beta} \lambda \right] z \right. \\ & \left. + \left[(\gamma - 1) + \left(\frac{1}{2} - \gamma + \beta \right) \Delta_{t,N\beta} \lambda \right] \right) \bar{\mathbf{u}}(z) = 0 \end{aligned} \quad (18)$$

with zeros

$$z = \frac{1 - 2\gamma + (1/2 + \gamma - 2\beta) \Delta_{t,N\beta} \lambda}{2\gamma + 2\beta \Delta_{t,N\beta} \lambda} \pm \frac{\sqrt{1 + (1 - 2\gamma) \Delta_{t,N\beta} \lambda + [(1/2 + \gamma)^2 - 4\beta] (\Delta_{t,N\beta} \lambda)^2}}{2\gamma + 2\beta \Delta_{t,N\beta} \lambda}. \quad (19)$$

The parameters γ and β must be chosen to have the desired accuracy and stability characteristics for a given time step of size $\Delta_{t,N\beta}$. For a time stepping scheme to be unconditionally stable, $|z| \leq 1$ for all $\Delta_{t,N\beta}$. This leaves the characterization of the eigenvalue λ of the coupled Maxwell system, which will be shown to have a nonnegative real part.

3.4.1. Eigenanalysis of System with Dirichlet and Impedance Boundary Conditions

The zeros of the stability equation values depend on the parameters γ and β , the time step size $\Delta_{t,N\beta}$, and the eigenvalues of the matrix system. First, consider a system with no impedance boundary conditions. The coupled Maxwell system can be analyzed by forming the generalized eigenvalue system

$$\mathbf{A}_1^{-1} \mathbf{A}_0 \begin{bmatrix} \bar{\mathbf{b}} \\ \bar{\mathbf{e}} \end{bmatrix} = \begin{bmatrix} 0 & \mathbf{D}_c \\ -\mathbf{M}_\varepsilon^{-1} \mathbf{D}_c^T \mathbf{M}_{\mu^{-1}} & 0 \end{bmatrix} \begin{bmatrix} \bar{\mathbf{b}} \\ \bar{\mathbf{e}} \end{bmatrix} = \lambda \begin{bmatrix} \bar{\mathbf{b}} \\ \bar{\mathbf{e}} \end{bmatrix}, \quad (20)$$

which leads to

$$\mathbf{D}_c \bar{\mathbf{e}} = \lambda \bar{\mathbf{b}}, \tag{21a}$$

$$-\mathbf{M}_\varepsilon^{-1} \mathbf{D}_c^T \mathbf{M}_{\mu^{-1}} \bar{\mathbf{b}} = \lambda \bar{\mathbf{e}}. \tag{21b}$$

It follows that

$$\mathbf{D}_c \mathbf{M}_\varepsilon^{-1} \mathbf{D}_c^T \mathbf{M}_{\mu^{-1}} \bar{\mathbf{b}} = -\lambda^2 \bar{\mathbf{b}} = \Lambda \bar{\mathbf{b}} \tag{22a}$$

$$\mathbf{M}_\varepsilon^{-1} \mathbf{D}_c^T \mathbf{M}_{\mu^{-1}} \mathbf{D}_c \bar{\mathbf{e}} = -\lambda^2 \bar{\mathbf{e}} = \Lambda \bar{\mathbf{e}}. \tag{22b}$$

The eigenvalues λ of the system matrix $\mathbf{A}_1^{-1} \mathbf{A}_0$ are purely imaginary when there are no impedance boundary conditions. This fact can be used to simplify Eq. (19) to find values γ and β that will result in a stable time stepping scheme.

The eigenvalues of the system change when impedance boundary conditions are imposed. The eigenvalues of $\mathbf{A}_1^{-1} \mathbf{A}_0$ have nonnegative real parts with impedance boundary conditions. First, the matrices in Eq. (16) are redefined in a more general form,

$$\mathbf{A}_1 = \begin{bmatrix} \mathbf{M}_{\mu^{-1}} & 0 \\ 0 & \mathbf{M}_\varepsilon \end{bmatrix}, \quad \mathbf{A}_0 = \begin{bmatrix} 0 & \mu_0^{-1} \mathbf{M}_c \\ -\mu_0^{-1} \mathbf{M}_c^T & \mathbf{M}_I \end{bmatrix} \tag{23}$$

where the basis functions can be of any order. To determine the behaviour of $\mathbf{A}_1^{-1} \mathbf{A}_0$, we create a similar matrix $\mathbf{A}_s = \mathbf{F} \mathbf{A}_s \mathbf{F}^{-1}$, where $\mathbf{F} = \mathbf{A}_1^{-1}$, leading to

$$\mathbf{A}_s = \begin{bmatrix} 0 & -\mu_0^{-1} \mathbf{M}_{\varepsilon^{-\frac{1}{2}}} \mathbf{M}_c \mathbf{M}_\varepsilon^{-\frac{1}{2}} \\ \mu_0^{-1} \mathbf{M}_\varepsilon^{-\frac{1}{2}} \mathbf{M}_c^T \mathbf{M}_{\mu^{-1}} & \mathbf{M}_\varepsilon^{-\frac{1}{2}} \mathbf{M}_I \mathbf{M}_\varepsilon^{-\frac{1}{2}} \end{bmatrix}. \tag{24}$$

This matrix is a non-symmetric saddle point matrix, whose properties are discussed in Theorem 3.6 in [29]. The matrix \mathbf{A}_s can be proven to be positive semi-definite because the matrix \mathbf{M}_I is positive semi-definite. Therefore, the eigenvalues of \mathbf{A}_s , and by the properties of similar matrices $\mathbf{A}_1^{-1} \mathbf{A}_0$, have nonnegative real parts. This is demonstrated for the zeroth and second order vector basis functions for both Dirichlet and impedance boundary conditions in Figure 2. The eigenvalues for the Dirichlet case lie on the imaginary axis, while the impedance boundary condition case is symmetric about the real axis in right half plane. Knowing that the eigenvalues have nonnegative real parts, it is possible to find general regions of stability and conditions for which the Newmark-Beta time-stepping scheme is nondissipative. The scheme is unconditionally stable for $\gamma \geq 0.5$ and $\beta \geq \gamma/2$. When $\gamma = 0.5$, $\beta \geq 0.25$, $|z| = 1$ for all the possible eigenvalues of $\mathbf{A}_1^{-1} \mathbf{A}_0$, Eq. (17) forms a nondissipative time-stepping scheme, which is essential in many applications. When $\gamma = 0.5$ and $\beta = 0.25$ or $\beta = 0.5$, we obtain a Crank-Nicholson scheme, which is known to be unconditionally stable and second order. Other choices of γ and β lead to dissipative, yet still stable time stepping schemes.

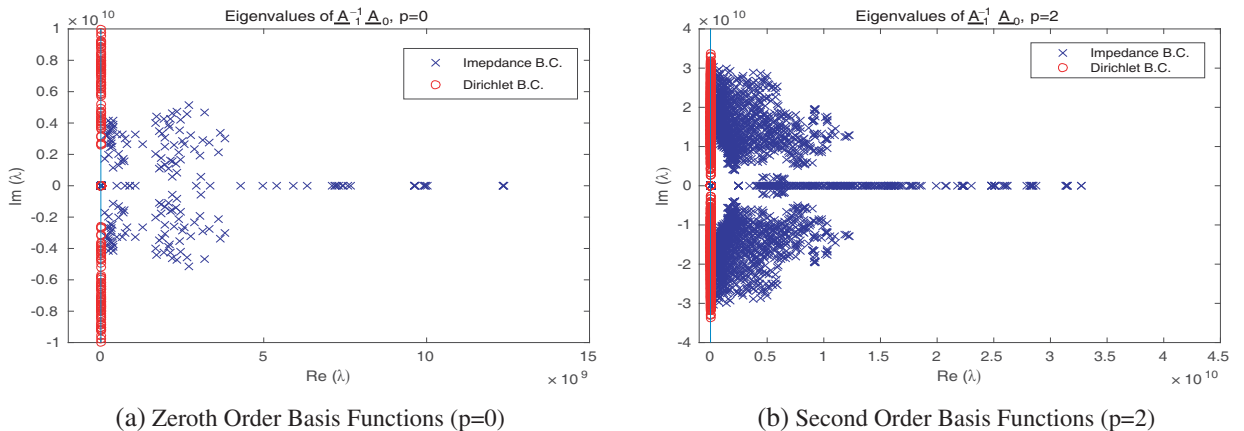


Figure 2. Eigenvalues of $\mathbf{A}_1^{-1} \mathbf{A}_0$.

4. RESULTS

In this section, we numerically demonstrate the utility of using the Newmark-Beta time stepping scheme with TD-MFEM. In particular, the resulting time stepping scheme is unconditionally stable while maintaining the convergence and accuracy properties of the more common leapfrog method.

4.1. Field Convergence

To numerically demonstrate convergence, a TEM plane wave is simulated propagating in free space normally incident through a $0.5 \text{ m} \times 0.5 \text{ m} \times 0.5 \text{ m}$ cube. The electric field of the plane wave is defined as

$$\bar{E}(\bar{r}, t) = \hat{y} \cos(2\pi f_0 t) e^{-(t-\bar{r}\cdot\hat{z}/c-8\sigma)^2/2\sigma^2} \text{ (V/m)}, \quad (25)$$

where $\sigma = 3/[2(f_{\max} - f_0)]$ with the center and maximum frequencies denoted as f_0 and f_{\max} , respectively. The relative error is defined as

$$\text{Relative Error} = \frac{\left\| \int d\Omega (\bar{\phi}_{\text{exp}}(\bar{r}, t) - \bar{\phi}_{\text{ana}}(\bar{r}, t)) \right\|_2}{\left\| \int d\Omega \bar{\phi}_{\text{ana}}(\bar{r}, t) \right\|_2} \quad (26)$$

where $\bar{\phi}(\bar{r}, t)$ can be either the electric field or magnetic flux density. The speed of propagation is the speed of light $c = 1/\sqrt{\epsilon\mu} = 1/\sqrt{\epsilon_0\mu_0}$ (m/s). Dirichlet boundary conditions as defined in Eq. (3) are used on each face of the volume, where $\bar{E}(\bar{r}, t)$ is defined in Eq. (25), and $\bar{B}(\bar{r}, t)$ follows from Maxwell's equations.

For the spatial convergence tests, the center frequency is 11 MHz, maximum frequency 21 MHz. Figure 3 shows the convergence properties of the fields with respect to space and basis function order. The convergence rates of the two time stepping schemes are the same, with similar errors as well. This is expected as the spatial discretization is the same. It is also noted that increasing the order of the basis function yields a greater improvement in accuracy than simply decreasing the element sizes.

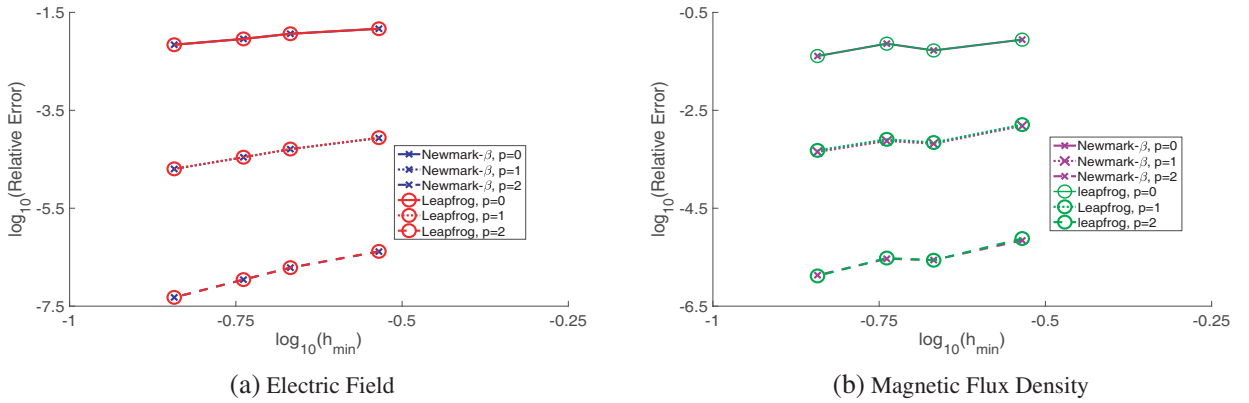


Figure 3. Space convergence.

Figure 4 shows the relative error in the electric field and magnetic flux as the time step size is changed using the Newmark-Beta time stepping scheme with $\gamma = 0.5$ and $\beta = 0.25$ for different orders of vector basis functions. The domain Ω is a $0.5 \text{ m} \times 0.5 \text{ m} \times 0.5 \text{ m}$ cube partitioned into 439 tetrahedra with an average edge length $h_{\text{avg}} = 143.7 \text{ mm}$. As the order of the Newmark-Beta time stepping scheme is the same as the Leapfrog scheme, it behaves similarly to the Newmark-Beta, but only for time step sizes smaller than the maximum time step size that is marked. Increasing the order of basis functions results in a smaller maximum time step size, whereas the unconditionally stable method allows for much larger time step sizes while maintaining the advantages of using higher order basis functions.

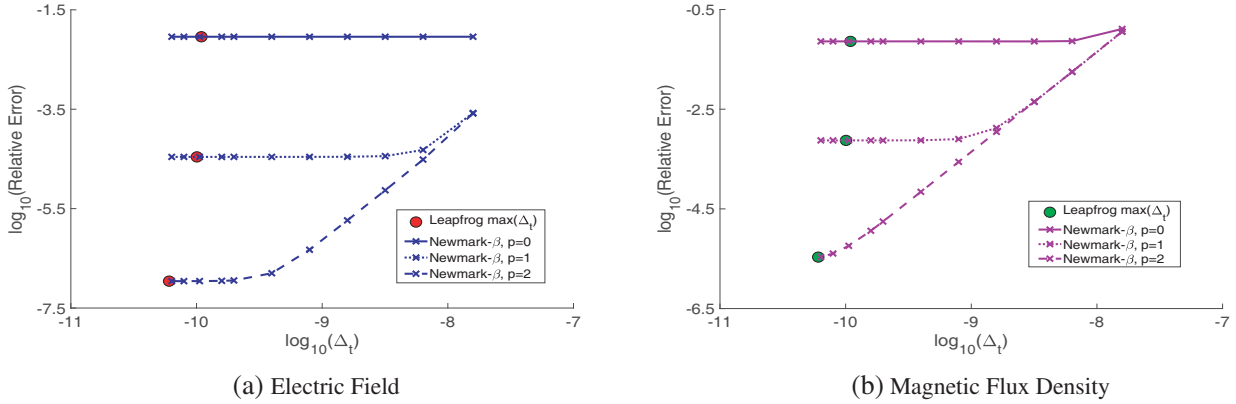


Figure 4. Time convergence.

4.2. Computational Cost Comparison

In the previous section, the spatial and temporal convergence of the Newmark-Beta time stepping scheme was compared to the leapfrog method. Here we compare the cost of using the Newmark-Beta time marching scheme. The leapfrog method requires matrix inversion for Eq. (13b). The Newmark-Beta method in Eq. (17) requires matrix inversion as well. The matrices in both Eqs. (13b) and (17) are sparse, having $\mathcal{O}(N_e)$ and $\mathcal{O}(N_e + N_f)$ nonzero elements, respectively. For practical problems, direct inversion is expensive, and iterative solvers are used instead. We assume that a Krylov subspace based method like GMRES converges in N_{iter} steps for both leapfrog and Newmark-Beta. Assuming that the duration of analysis is T gives $N_{t,lf}$ and $N_{t,N\beta}$ as the numbers of time steps for leapfrog and Newmark-Beta, respectively. It follows that runtime scales as $\mathcal{O}(N_{t,lf}N_{iter}N_e)$ for leapfrog and $\mathcal{O}(N_{t,N\beta}N_{iter}(N_e + N_f))$ for Newmark-Beta. It is apparent that the increased degree of freedom required for a Newmark system could lead to higher costs; however, the time step sizes can be vastly different. Indeed, depending on the geometry (especially when discretization is driven by the need to capture feature sizes), the cost of the increased degrees of freedom can be counterbalanced by the number of time steps taken when there is flexibility in the time step size. Thus, as the ceiling of $\Delta_{t,LF}$ is fixed by the mesh, so is the number of time steps for a fixed duration. However, this is not the case for Newmark-Beta. The numerical experiment conducted next illustrates the cost tradeoff.

This experiment is shown in Figure 5 and is conducted using three $1\text{ m} \times 1\text{ m} \times 1\text{ m}$ cubes with Dirichlet boundary conditions. A normally-incident TEM plane wave is simulated propagating in free space. The electric field is defined in Eq. (25) with a center frequency of 110 MHz and a maximum frequency of 210 MHz. The Newmark-Beta time stepping scheme was run three times for the same amount of simulated time. Once at the maximum time step size for leapfrog, once at half that time

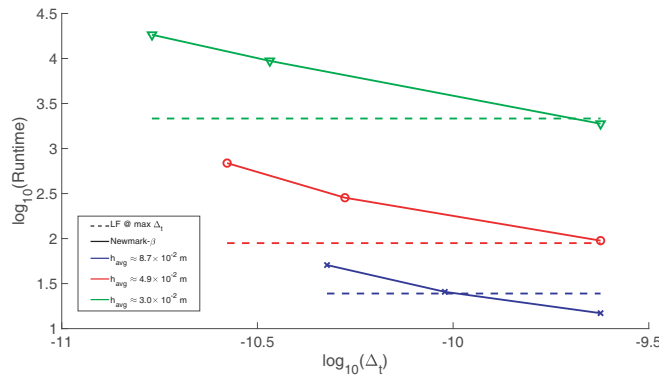


Figure 5. Runtime comparison.

step size, and once with a time step size of $1/20f_{\max} \approx 238$ ps. GMRES was used with a diagonal preconditioner and a tolerance of 10^{-4} . When $\Delta_{t,N\beta} = 1/20f_{\max}$, the runtime for Newmark-Beta was equal to or faster than leapfrog. While this was a simple example, we expect to reap significant benefits as the model representation drives discretization.

4.3. Eigenvalues of Space-Time matrix

In this test, we further verify the stability of the proposed Newmark-Beta time-marching scheme. To determine the stability of a time stepping schemes, we analyze the eigenvalues of a space-time matrix \mathbf{A} that satisfies

$$\bar{u}^{n+1} = \mathbf{A}\bar{u}^n \quad (27)$$

for some input vector \bar{u}_n . The space-time matrix is an amplification matrix for some input, and for it to have a bounded output, the absolute value of the eigenvalues must lie on or within the unit circle in the complex domain. For an energy-conserving system, all the eigenvalues lie on the unit circle, signifying that there is no numerical loss in the system. In this example, two different meshes discretize the same 1 m cube. The first mesh is nearly uniformly discretized, with a ratio of $h_{\max}/h_{\min} \approx 1.5$, where h is the edge length. The second mesh is not uniformly discretized, in which the edges become smaller near one face. The ratio of the largest edge to smallest edge in the nonuniform mesh is ≈ 8 . Figures 6, 7, and 8 compare the eigenvalues of the space-time matrices for both the leapfrog and Newmark-Beta time stepping schemes for varying time step size. The reference time step size $\Delta_t = 1/(30f_{\max})$.

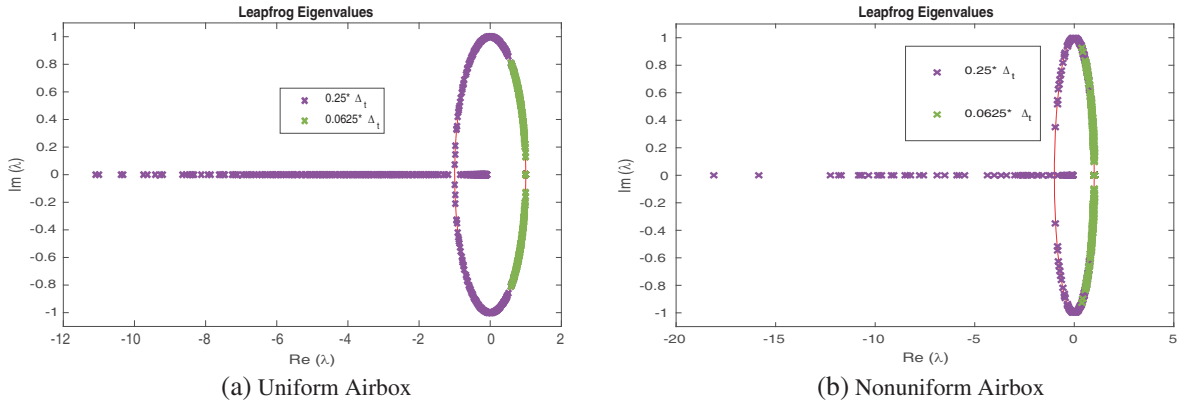


Figure 6. Leapfrog eigenvalues.

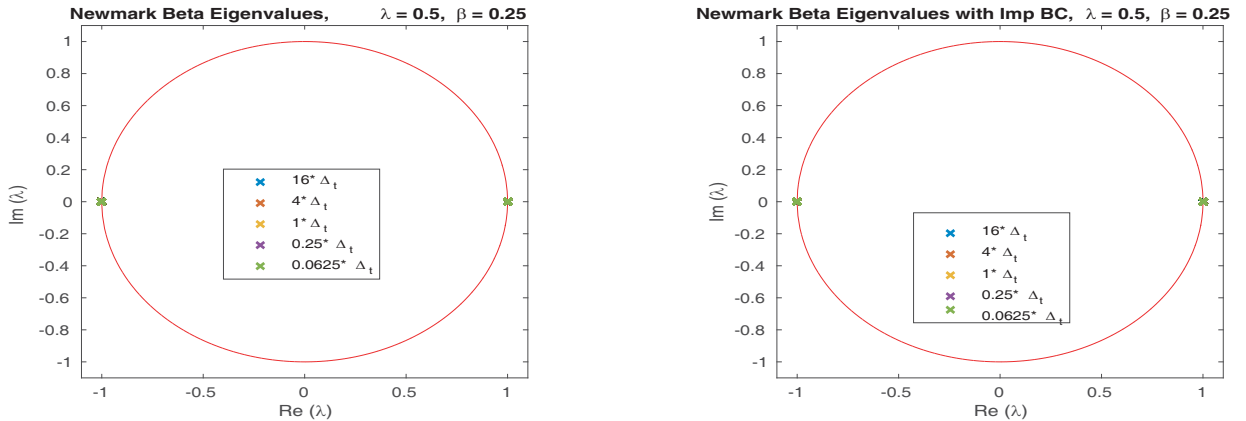


Figure 7. Newmark-Beta eigenvalues for uniform airbox.

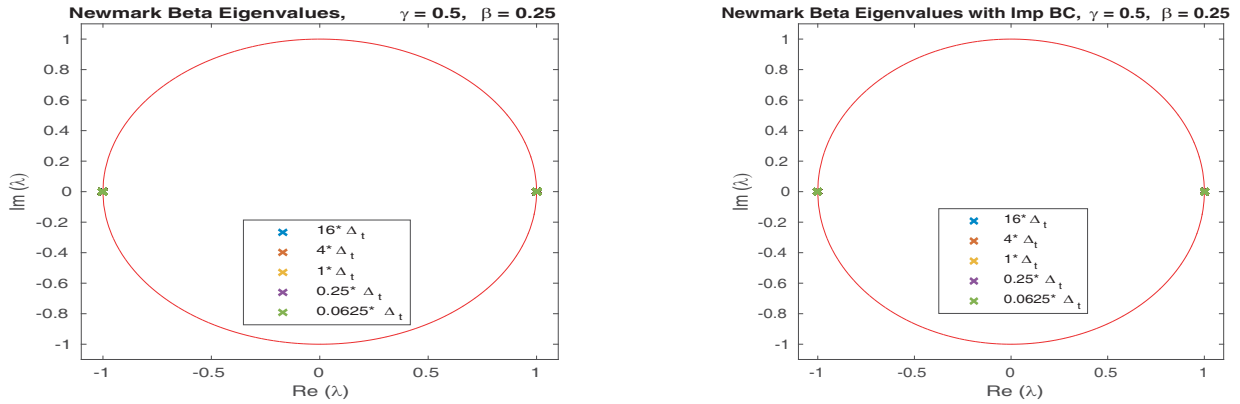
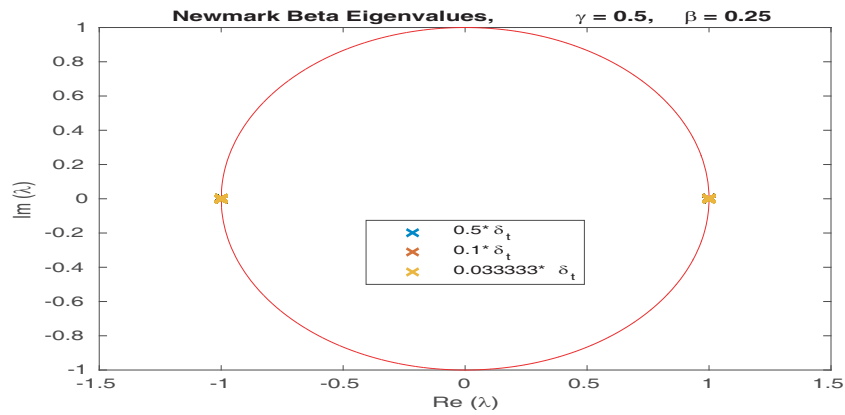
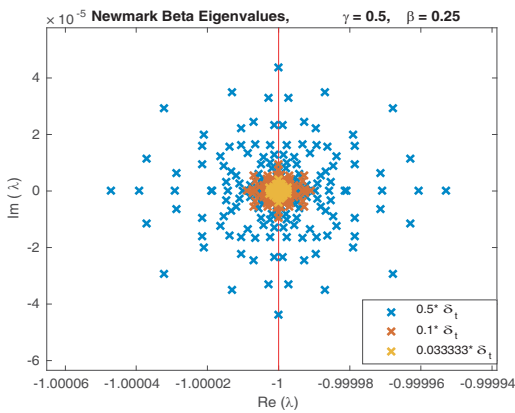


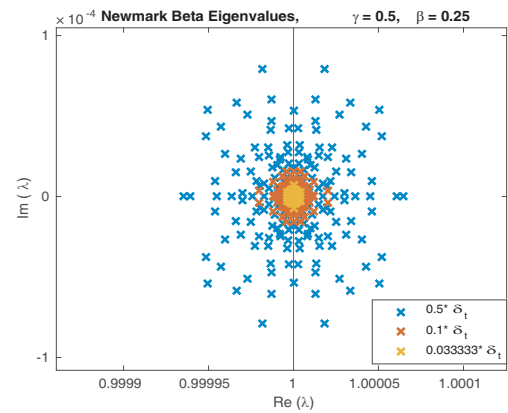
Figure 8. Newmark-Beta eigenvalues for nonuniform airbox.



(a) First Order



(b) $p=1$, Centered at $Re(\lambda) = -1$



(c) $p=1$, Centered at $Re(\lambda) = 1$

Figure 9. Newmark-Beta eigenvalues for uniform airbox with first order basis functions.

When the time step size of the leapfrog method satisfies the stability criterion, the eigenvalues all lie on the unit circle. However, when the time step size no longer satisfies the stability criterion, the eigenvalues close to -1 leave the unit circle and head toward 0 and $-\infty$.

Figures 7 and 8 show that the space-time eigenvalues of the Newmark-Beta time stepping scheme with $\gamma = 0.5$ and $\beta = 0.25$ always lie on the unit circle for a wide range of time step sizes, lending credence to its unconditionally stable nature. The eigenvalues of the system when these particular values

are chosen are analytically ± 1 . Figure 7 uses the uniformly discretized volume, and Figure 8 uses the nonuniformly discretized volume, with both showing the behavior with Dirichlet boundary conditions and impedance boundary conditions. As the overall eigenvalue behavior holds as the basis function order increases, similar results are seen in Figures 9 and 10, which shows the space-time eigenvalues of the same uniform airbox with Dirichlet boundary conditions, but with first and second order basis

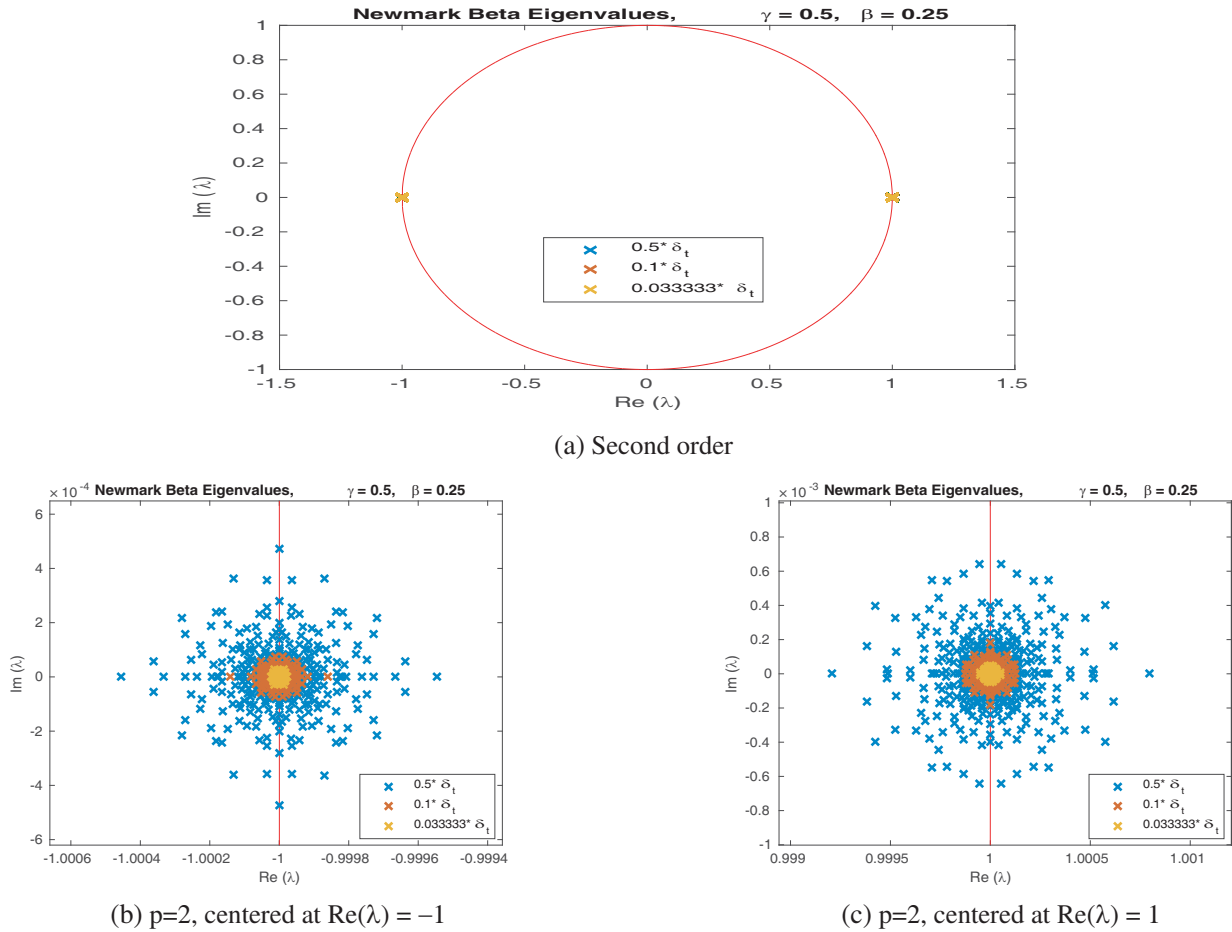


Figure 10. Newmark-Beta eigenvalues for uniform airbox with second order basis functions.

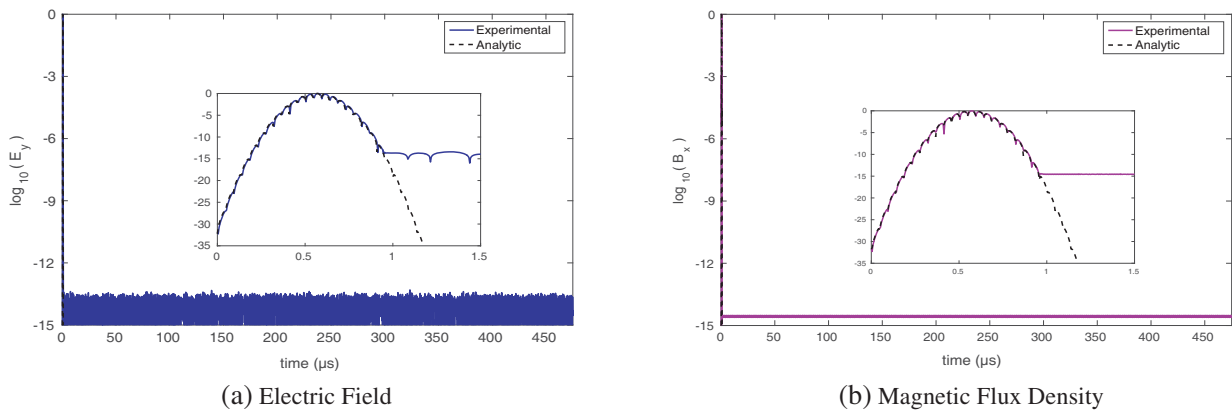


Figure 11. Plane wave simulation for 100,000 time steps.

functions. Closer inspection of the eigenvalues show that there is an error, as the eigenvalues lie outside the unit circle, but it is strictly numerical in nature and related to the condition number of the matrix $\mathbf{A}_1^{-1}\mathbf{A}_0$.

Finally, to numerically confirm late-time stability, Figure 11 shows the electric field and magnetic flux density run for 100,000 time steps at a time step size of $\Delta_{t,N\beta} = 1/10f_{\max}$ or 4.762 ns. There is a noise floor that corresponds to a DC null space. However, the noise does not grow over time, indicating that the nullspace does not contain $t\nabla\phi(\bar{r})$ present in TD-FEM.

5. SUMMARY

In this work, it was proven that the Newmark-Beta algorithm can be used to create an unconditionally stable time stepping framework for solving TD-MFEM. We proved stability for systems arising from different boundary conditions, as well as showed convergence and energy conservation. The benefit of being able to use different time step sizes is apparent. In future work, this method will be applied to simulating plasmas. Utilizing higher order basis sets with optimal particle pushing strategies will be investigated. Preconditioning strategies will also be developed to improve the use of iterative solvers for TD-MFEMs.

ACKNOWLEDGMENT

This work was supported by the Department of Energy Computational Science Graduate fellowship under grant DE-FG02-97ER25308. The authors were also supported in part by the HPCC Facility at Michigan State University under Grant NSF ECCS-1408115, and AFOSR Grant RC107859.

REFERENCES

1. Jin, J.-M. and D. J. Riley, *Finite Element Analysis of Antennas and Arrays*, Wiley Online Library, 2009.
2. Saitoh, K. and M. Koshiba, "Full-vectorial imaginary-distance beam propagation method based on a finite element scheme: Application to photonic crystal fibers," *IEEE Journal of Quantum Electronics*, Vol. 38, No. 7, 927–933, 2002.
3. Fivaz, M., S. Brunner, G. de Ridder, O. Sauter, T. Tran, J. Vaclavik, L. Villard, and K. Appert, "Finite element approach to global gyrokinetic particle-in-cell simulations using magnetic coordinates," *Computer Physics Communications*, Vol. 111, No. 1, 27–47, 1998.
4. Lee, J.-F., D.-K. Sun, and Z. J. Cendes, "Full-wave analysis of dielectric waveguides using tangential vector finite elements," *IEEE Transactions on Microwave Theory and Techniques*, Vol. 39, No. 8, 1262–1271, 1991.
5. Rahman, B. A. and J. B. Davies, "Finite-element analysis of optical and microwave waveguide problems," *IEEE Transactions on Microwave Theory and Techniques*, Vol. 32, No. 1, 20–28, 1984.
6. Yee, K. S. and J. S. Chen, "The finite-difference time-domain (FDTD) and the finite-volume time-domain (FVTD) methods in solving Maxwell's equations," *IEEE Transactions on Antennas and Propagation*, Vol. 45, No. 3, 354–363, 1997.
7. Cendes, Z. J., "Vector finite elements for electromagnetic field computation," *IEEE Transactions on Magnetics*, Vol. 27, No. 5, 3958–3966, 1991.
8. Lee, J.-F., R. Lee, and A. Cangellaris, "Time-domain finite-element methods," *IEEE Transactions on Antennas and Propagation*, Vol. 45, No. 3, 430–442, 1997.
9. Monk, P., et al., *Finite Element Methods for Maxwell's Equations*, Oxford University Press, 2003.
10. Jin, J.-M., *The Finite Element Method in Electromagnetics*, John Wiley & Sons, 2015.
11. Graglia, R. D., D. R. Wilton, and A. F. Peterson, "Higher order interpolatory vector bases for computational electromagnetics," *IEEE Transactions on Antennas and Propagation*, Vol. 45, No. 3, 329–342, 1997.

12. Graglia, R. D. and A. F. Peterson, "Hierarchical divergence-conforming Nédélec elements for volumetric cells," *IEEE Transactions on Antennas and Propagation*, Vol. 60, No. 11, 5215–5227, 2012.
13. Lee, S.-C., M. N. Vouvakis, and J.-F. Lee, "A non-overlapping domain decomposition method with nonmatching grids for modeling large finite antenna arrays," *Journal of Computational Physics*, Vol. 203, No. 1, 1–21, 2005.
14. Gedney, S. D. and U. Navsariwala, "An unconditionally stable finite element time-domain solution of the vector wave equation," *IEEE Microwave and Guided Wave Letters*, Vol. 5, No. 10, 332–334, 1995.
15. Rylander, T. and A. Bondeson, "Stability of explicit-implicit hybrid time-stepping schemes for Maxwell's equations," *Journal of Computational Physics*, Vol. 179, No. 2, 426–438, 2002.
16. Bossavit, A., "Whitney forms: A class of finite elements for three-dimensional computations in electromagnetism," *IEE Proceedings A — Physical Science, Measurement and Instrumentation, Management and Education — Reviews*, Vol. 135, No. 8, 493–500, 1988.
17. Bossavit, A. and L. Kettunen, "Yee-like schemes on a tetrahedral mesh, with diagonal lumping," *International Journal of Numerical Modelling: Electronic Networks, Devices and Fields*, Vol. 12, Nos. 1–2, 129–142, 1999.
18. Wong, M.-F., O. Picon, and V. F. Hanna, "A finite element method based on whitney forms to solve Maxwell equations in the time domain," *IEEE Transactions on Magnetics*, Vol. 31, No. 3, 1618–1621, 1995.
19. Rodrigue, G. and D. White, "A vector finite element time-domain method for solving Maxwell's equations on unstructured hexahedral grids," *SIAM Journal on Scientific Computing*, Vol. 23, No. 3, 683–706, 2001.
20. Akbarzadeh-Sharbat, A. and D. D. Giannacopoulos, "Finite-element time-domain solution of the vector wave equation in doubly dispersive media using Möbius transformation technique," *IEEE Transactions on Antennas and Propagation*, Vol. 61, No. 8, 4158–4166, 2013.
21. Tarhasaari, T., L. Kettunen, and A. Bossavit, "Some realizations of a discrete Hodge operator: A reinterpretation of finite element techniques [for EM field analysis]," *IEEE Transactions on Magnetics*, Vol. 35, No. 3, 1494–1497, 1999.
22. Teixeira, F. L. and W. C. Chew, "Lattice electromagnetic theory from a topological viewpoint," *Journal of Mathematical Physics*, Vol. 40, No. 1, 169–187, 1999.
23. Gedney, S. D. and J. A. Roden, "Numerical stability of nonorthogonal FDTD methods," *IEEE Transactions on Antennas and Propagation*, Vol. 48, No. 2, 231–239, 2000.
24. Wang, S. and F. L. Teixeira, "Some remarks on the stability of time-domain electromagnetic simulations," *IEEE Transactions on Antennas and Propagation*, Vol. 52, No. 3, 895–898, 2004.
25. Newmark, N. M., "Computation of dynamic structural response in the range approaching failure," Department of Civil Engineering, University of Illinois, 1952.
26. Wood, W. L., *Practical Time-stepping Schemes*, Clarendon Press, Oxford University Press, Oxford, New York, England, 1990.
27. Zienkiewicz, O. C., "A new look at the newmark, houbolt and other time stepping formulas. A weighted residual approach," *Earthquake Engineering & Structural Dynamics*, Vol. 5, No. 4, 413–418, 1977.
28. Zienkiewicz, O. C. and K. Morgan, *Finite Elements and Approximation*, Wiley, New York, 1983.
29. Benzi, M., G. H. Golub, and J. Liesen, "Numerical solution of saddle point problems," *Acta Numerica*, Vol. 14, 1–137, 2005.